ACS Catalysis

pubs.acs.org/acscatalysis Research Article

Catalytic Activity of Aliphatic PNP Ligated $Co^{III/I}$ Amine and Amido Complexes in Hydrogenation Reaction—Structure, Stability, and Substrate Dependence

Jiali Liu, Zhihong Wei,* and Haijun Jiao*

Cite This: ACS Catal. 2021, 11, 4593−4605 Read Online

ACCESS | Metrics & More | Article Recommendations | SI Supporting Information

ABSTRACT: Structures, energies, and stability of aliphatic PNP ligated Co^{III}/Co^{I} amine and amido complexes in different spin (singlet, triplet, and open-shell singlet) states and coordination spheres have been computed. Spin exchange is found for the interconversion between the singlet Co^{III} amine and the triplet Co^{I} amine complexes as well as the singlet Co^{III} amido and the triplet Co^{I} amido complexes. For the hydrogenation of CH_2O, PhCHO, and $PhCOCH_3$ having lower Gibbs free energy barriers than that of the interconversion from the singlet Co^{III} amine and the triplet Co^{I} amine complexes, both singlet Co^{III} amine and triplet Co^{I} amine complexes are active catalysts and both catalytic cycles are independent, and the triplet Co^{I} amine complex is more active than the singlet Co^{III} amine complex. For the hydrogenation of $PhCOOCH_3$ having higher barrier than that of catalyst interconversion, the singlet Co^{III} amine complex is the sole active catalyst and more active than the triplet Co^{I} amine complex. For the hydrogenation of CH_3COCH_3, both catalytic cycles can be competitive depending on reaction temperature. These reveal the substrate dependent mechanisms. The correlation between the hydride affinity of the substrate and the H^- transfer barrier for aldehydes and ketones as well as between the deprotonation energy of alcohol and the reverse barrier of H^+ transfer indicates that the energy of the transition state of the H^-/H^+ transfer via the corresponding most favorable mechanism can be estimated by the hydride affinity of substrate and the deprotonation energy of the product.

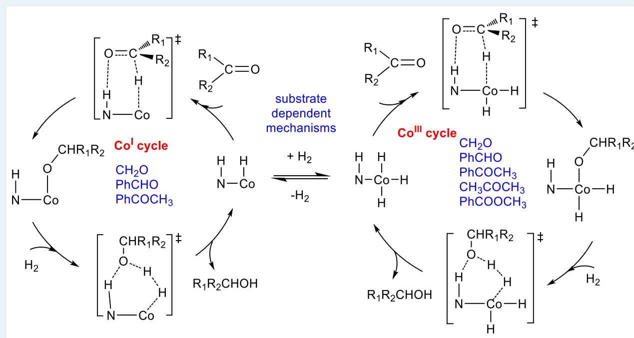

KEYWORDS: *Co^{III}/Co^{I} complexes, PNP ligands, stability, spin states, interconversion, catalysis, hydrogenation*

INTRODUCTION

Homogeneous hydrogenation reaction, which enables selective transformation of unsaturated substrates into desired products under mild conditions,[1,2] represents one of the most important methodologies in academic research and industrial applications. To fulfill the principle of sustainable and green chemistry as well as economical investment, current research focus has shifted to earth-abundant 3d transitional metals, although traditional noble transition metal complexes exhibit excellent catalytic activities in hydrogenation processes.[3−6] With respect to the milestone work of Shvo and Noyori in metal−ligand bifunctional catalysis,[7−9] catalytic hydrogenation and dehydrogenation with bifunctional complexes have been widely explored and applied.[10−16] Among them, tridentate pincer ligated metal complexes bearing bifunctional site for reversible protonation and deprotonation interconversion via the embedded nitrogen in aromatic pyridine $PN_{py}P$ $[NC_5H_3(CH_2PR_2)_2]$ or aliphatic amine PNP $[HN(CH_2CH_2PR_2)_2]$ ligands have been proven as effective catalysts for reactions involving hydrogenation and dehydrogenation steps.[17−19] Recent studies proved that pincer ligated complexes bearing similar ligand and coordination frameworks provide an opportunity for replacing noble metals by base metals. The most extensively tested candidates for reactions involving hydrogenation and dehydrogenation steps are Fe[18,20−24] and Mn[19,25,26] based PNP complexes. These complexes show excellent catalytic activities in the hydrogenation of nitriles, imines, alkenes, transfer hydrogenation of carbonyl compounds, acceptor-less dehydrogenative coupling of alcohols to esters/amides, and aqueous methanol dehydrogenation which includes formic acid dehydrogenation in the last step to H_2 and CO_2.[12,17,26,27] Besides Fe and Mn PNP pincer complexes, Co PNP pincer complexes are attracting increasing attention.[12,26,28,29] However, Co PNP complexes are much more complicated due to their different oxidation and spin states via electron transfer and/or different coordination environment.[30,31] Scheme 1 (top) shows the interconversion of Co-

Received: December 18, 2020
Revised: March 21, 2021
Published: March 31, 2021

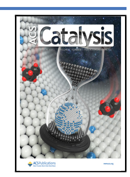

Scheme 1. Reported Co Pincer Complexes in Exchangeable Oxidation States

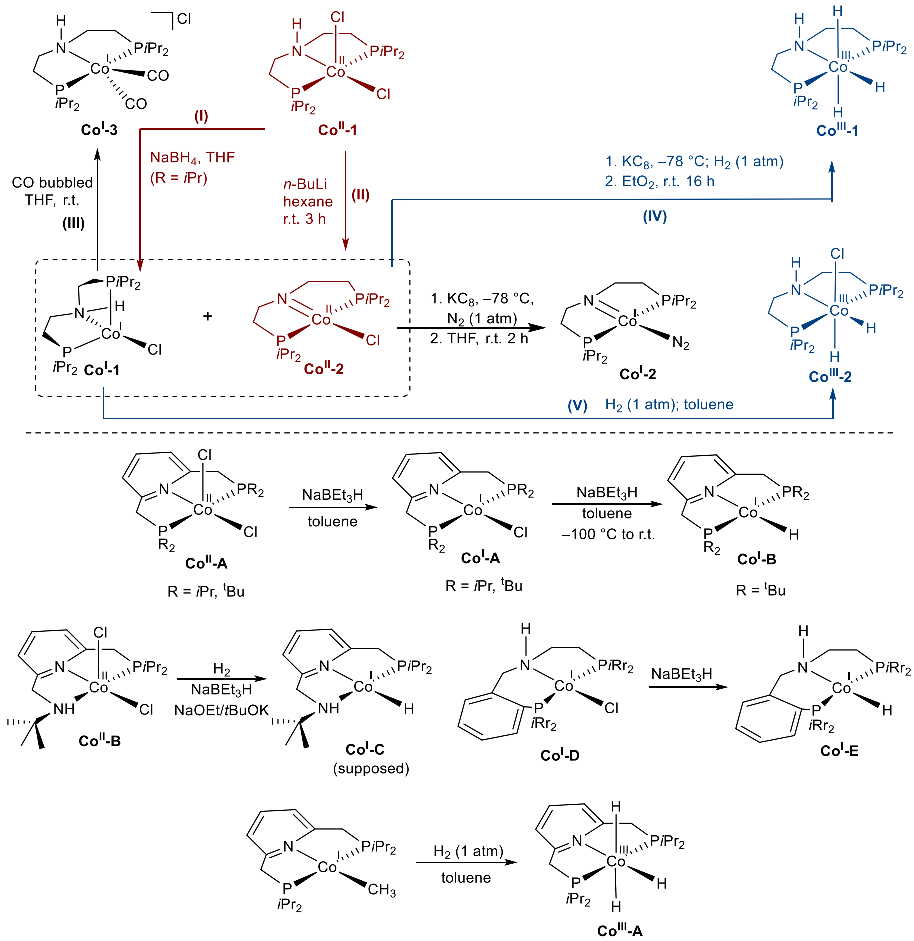

complexes in different oxidation states under different reaction conditions (**I**,[32] **II**,[33] **III**,[33,34] **IV**, and **V**[35]), and this complexity makes the experimental identification and characterization of active Co species as well as mechanistic study difficult.

In recent years, scientists explored the possible real catalysts when utilizing other cobalt pincer complexes. Relative systems and reactions are outlined in Scheme 1 (bottom). The Chirik group validated that monovalent cobalt complexes [(PNP)-Co^{I}Cl] (**Co^{I}−A**) and [(PNP)Co^{I}H] (**Co^{I}−B**) are generated when applying 1 and 2 equiv of NaHBEt$_3$ with [(PNP)-Co^{II}(Cl)$_2$] (**Co^{II}−A**).[36,37] Milstein and co-workers inferred that an in situ monovalent cobalt hydride [(PNNH)Co^{I}H] (**Co^{I}−C**) complex is the active catalyst under the reaction conditions when applying the [(PNNH)Co^{II}(Cl)$_2$] (**Co^{II}−B**) complex as the precatalyst in the hydrogenation of esters,[38] dehydrogenative coupling of diols and amines,[39] and selective hydrogenation of nitriles to primary amines.[40] In addition, the isolated paramagnetic species, possibly [(*i*Pr-PN^{H}P)Co^{I}H] (**Co^{I}−E**), is generated when treating [(*i*Pr-PN^{H}P)Co^{I}Cl] (**Co^{I}−D**) with 1 equiv of NaBEt$_3$H. Furthermore, the Co−H stretching frequency is displayed in IR spectrum and possible complexes [(*i*Pr-PN^{H}P)Co^{I}H] shows perfect catalytic activity without base additive.[41] Sandip found that the Co−H bond may play an important role in the selective hydrogenation of esters to aldehydes and alcohols, and this hydrogenation reaction involves metal−ligand cooperation.[42] Monochloro species [(PNP)Co^{I}Cl] (**Co^{I}−1**) shows excellent catalytic activity in the hydrogenation of methyl benzoate, indicating that the monovalent or trivalent hydride complex is the possible active species.[32] In 2011, Yang predicted the trivalent complex [(PNP)Co^{III}(H)$_3$] (**Co^{III}−A**) as a potential computationally active catalyst.[43] Furthermore, Chirik's group identified the trihydride cobalt complex **Co^{III}−A**, which can easily give a reductive product once the H$_2$ atmosphere is removed.[36] In addition, a trivalent cobalt complex [(HPNP)Co^{III}(H)$_3$] (**Co^{III}−1**) is produced when treating [(PNP)Co^{I}Cl] (**Co^{I}−1**) with KC$_8$ under H$_2$ atmosphere via oxidative addition and different orientations of the PNP-backbone have a great influence on the stability of **Co^{III}−1**.[35] Studying catalysts under reaction conditions challenge not only experiment but also computation. Even problematic is the minimum energy path involving spin exchange among the singlet, triplet, and open-shell singlet states on the Gibbs free energy profiles.[44,45]

Such complexities, however, provide opportunities for unprecedented coordination chemistry, distinct mechanistic pathways, and unique activities. Despite difficulties in identifying and characterizing active species from experiments, it is important to study Co PNP active catalysts for understanding its stability and interconversion in different oxidation states, spin states and geometries. To the best of our knowledge, there are no such systematic studies focusing on structural analysis and a full reaction network for aliphatic Co PNP species interconversion. In catalytic reactions, both inner-sphere and outer-sphere mechanisms as well as innocent and noninnocent mechanisms of the ligand were proposed for Co PNP catalyzed (de)hydrogenation for specific substrates,

https://doi.org/10.1021/acscatal.0c05562
ACS Catal. 2021, 11, 4593−4605

however, whether these mechanisms are competitive or exchangeable need to be investigated. In this work, we computed the interconversion among the Co^{III}/Co^{I} amine and amido hydride cobalt complexes to understand its stability, spin states, and geometries. Further, we investigated their thermal stability and interconversion of Co^{I}–, Co^{III}–amine, and amido complexes as well as the hydrogenation mechanisms of aldehydes (CH_2O, PhCHO), ketones (CH_3COCH_3, $PhCOCH_3$), and ester ($PhCOOCH_3$). The experimentally reported studies of the hydrogenation of aldehydes and ketones,[34] the acceptor-less dehydrogenation of secondary alcohols[46] and the hydrogenation of carboxylic esters[31,32] using different well-defined Co-PNP pincer complexes were shown in Scheme 2. The reactivity and properties of the catalyst and substrate were correlated. We expect that this study will be helpful for the optimization of reaction parameters and catalyst design.

Scheme 2. Co PNP Catalyzed Hydrogenation of Aldehydes, Ketones,[34] and Carboxylic Esters,[31,32] as well as Acceptor-Dehydrogenation of Secondary Alcohols[46]

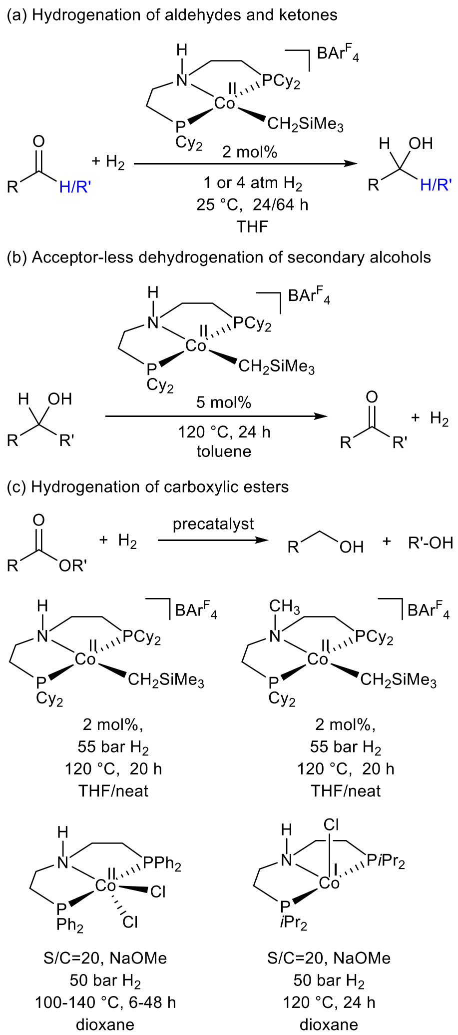

■ COMPUTATIONAL METHODS

All geometry optimization and frequency analysis of reactants, intermediates, and transition states were performed using the Gaussian 16 program.[47] Aiming to find the most suitable level in our reaction system, we tested a couple of common functional used in organometallic catalytic systems along with the TZVP[48] basis set in the gas phase. Frequency calculations were performed for all optimized structures with only one imaginary frequency for transition states and only real frequencies for minimum structures. Considering the specific reaction conditions, we carried out geometry optimization and the corresponding frequencies in 1,4-dioxane solution based on solute electron density (SMD[49]). The benchmark test in solution shows that the M06-L[50] functional has a minimum deviation from the experimental thermodynamic data (Figure S1 of the Supporting Information, SI). We used the corrected Gibbs free energy at 298 K and 1 atm derived from the frequency analysis in solution for our discussion and analysis. The Gibbs free energy in black (or ^{1}**a**) denotes singlet states, in red (or ^{3}**a**) displays triplet states and in purple (or ^{OS}**a**) is used for open-shell singlet states.

■ RESULTS AND DISCUSSION

Stability and Interconversion of Co^{I}–, Co^{III}–Amine, and Amido Complexes. *Minimum Energy Path for the Interconversion Co^{I}–, Co^{III}–Amine, and Amido Complexes.* The full Gibbs free energy profile with all transition states and intermediates are given in the SI (Figure S2) and the minimum energy path is shown in Figure 1. It is found that both Co^{III} amine and amido complexes have closed-shell singlet ground states, due to their 18-valence-electron configurations. Moreover, the triplet state is the ground state for the monovalent Co^{I} complexes. Starting from the most stable singlet ^{1}**2Co^{III}** amine complex, the interconversion to the singlet ^{1}**1Co^{III}** amido complex prefers a concerted transition state with a Gibbs free energy barrier of 100.7 kJ/mol via ^{1}**TS–H$_2$–Co^{III}** and is endergonic by 27.2 kJ/mol. For the amine complex (**2Co^{I}**), we computed a twisted structure in C_1 symmetry (**2Co$^{I}_{dist}$**) and a C_s symmetrical isomer (**2Co^{I}**/C_s). It is found that both isomers have triplet ground states, and the twisted C_1 form is more stable than the C_s form by 10.7 kJ/mol. In 2013, Arnold's group found that [$Co^{I}Cl(HN(CH_2CH_2PiPr_2)_2)$] possess two unpaired electrons,[33] which coincides with the triplet ground state of ^{3}**2Co^{I}**. Therefore, we defined the most stable twisted C_1 form in triplet ground state (^{3}**2Co$^{I}_{dist}$**) as ^{3}**2Co^{I}** for our calculation. The interconversion from singlet ^{1}**2Co^{III}** to the singlet ^{1}**2Co^{I}** amine complex possesse a most favorable transition state ^{1}**TS–OA2** with a barrier of 84.2 kJ/mol and is endergonic by 67.4 kJ/mol. However, it is noted that the singlet ^{1}**2Co^{I}** amine complex is less stable than the corresponding triplet state and spin exchange takes place and is exergonic by 38.4 kJ/mol. Compared with the interconversion between ^{1}**2Co^{III}** and ^{1}**1Co^{III}**, that between ^{1}**2Co^{III}** and ^{3}**2Co^{I}** has lower barrier (84.2 vs 100.7 kJ/mol) and is closely endergonic (29.0 vs 27.2 kJ/mol), revealing their thermodynamic competition. However, spin exchange from the singlet amine ^{1}**2Co^{III}** to the triplet amine ^{3}**2Co^{I}** should take place after the transition state. On the basis of the coordination environment and for the hydrogenation reactions, the singlet ^{1}**1Co^{III}** amido complex should prefer outer-sphere mechanism, while the triplet ^{3}**2Co^{I}** amine complex should favor the inner-sphere mechanism. However, these require both experimental and computational evidence and confirmation.

Starting from the ^{3}**2Co^{I}** amine complex, it is possible to go through transition state ^{3}**TS–H$_2$–Co^{I}** generating the corresponding ground state ^{3}**1Co^{I}** amido complex; and this interconversion has a barrier of 86.7 kJ/mol and is endergonic

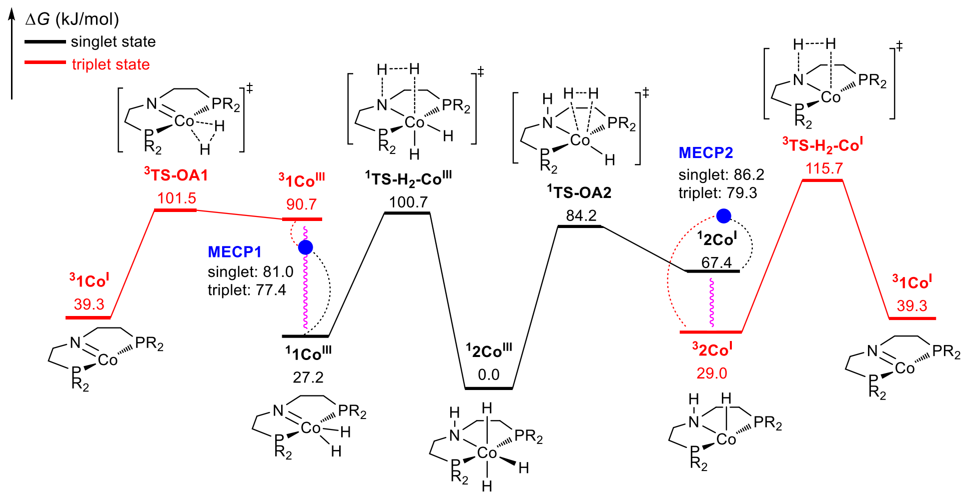

Figure 1. Minimum energy path of the Co^{III} and Co^{I} complexes interconversion (R = isopropyl).

Scheme 3. Proposed Mechanisms of Co^{III} Catalyzed C=O Hydrogenation

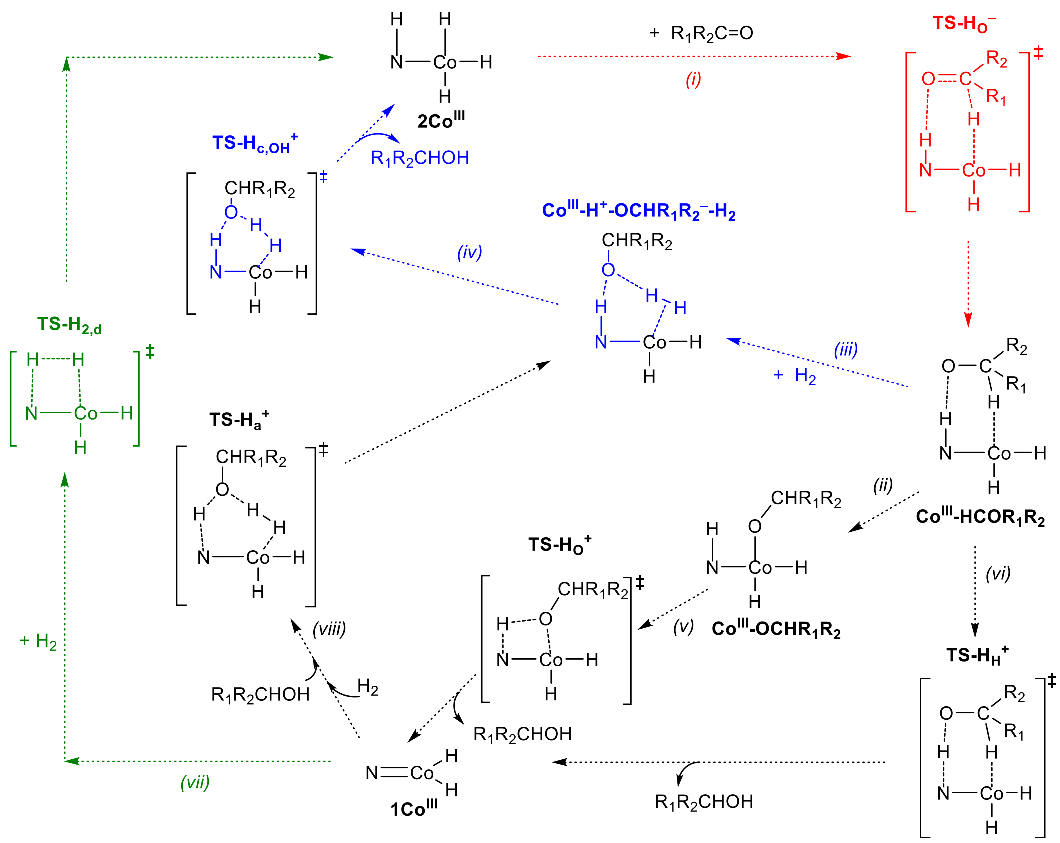

by 10.3 kJ/mol. Compared with the interconversion between ^{1}**2Co**^{III} and ^{1}**1Co**^{III}, the interconversion between ^{3}**2Co**^{I} and ^{3}**1Co**^{I} has lower barrier (86.7 vs 100.7 kJ/mol) and is less endergonic (10.3 vs 27.2 kJ/mol), revealing that trivalent Co^{III} and monovalent Co^{I} complexes should have different stability and activity. On the contrary, the interconversion from the singlet ^{1}**1Co**^{III} amido complex to the triplet ^{3}**1Co**^{I} amido complex needs spin exchange at first, i.e., from the singlet ^{1}**1Co**^{III} to the triplet ^{3}**1Co**^{III} of being endergonic by 63.5 kJ/mol; and has a total barrier of 74.3 kJ/mol and is endergonic by 12.1 kJ/mol. In addition, we searched the minimum energy crossing point (MECP) by using the same method[45] and program (sobMECP).[51,52] The respective thermal correction to Gibbs free energy for the optimized MECPs was calculated by using projected frequency analysis in different spin states.[53] All relative data are given in Table S2 and the MECPs are shown in Figure 1. For the spin-crossing from the singlet ^{1}**1Co**^{III} to the triplet ^{3}**1Co**^{III}, singlet ^{1}**1Co**^{III} transforms to triplet ^{3}**1Co**^{III} via the MECP1 (81.0 kJ/mol). For the spin-crossing between from the singlet^{1}**2Co**^{I} to the triplet ^{3}**2Co**^{I}, singlet state of ^{1}**2Co**^{I} converts to triplet state of ^{3}**2Co**^{I} via MECP2 (86.2 kJ/mol). It is also noted that for MECP1, the Gibbs free energy difference and the difference of total electronic energy are close (53.8 vs 64.1 kJ/

https://doi.org/10.1021/acscatal.0c05562
ACS Catal. 2021, 11, 4593−4605

Scheme 4. Proposed Mechanism of Co^I Catalyzed C═O Hydrogenation

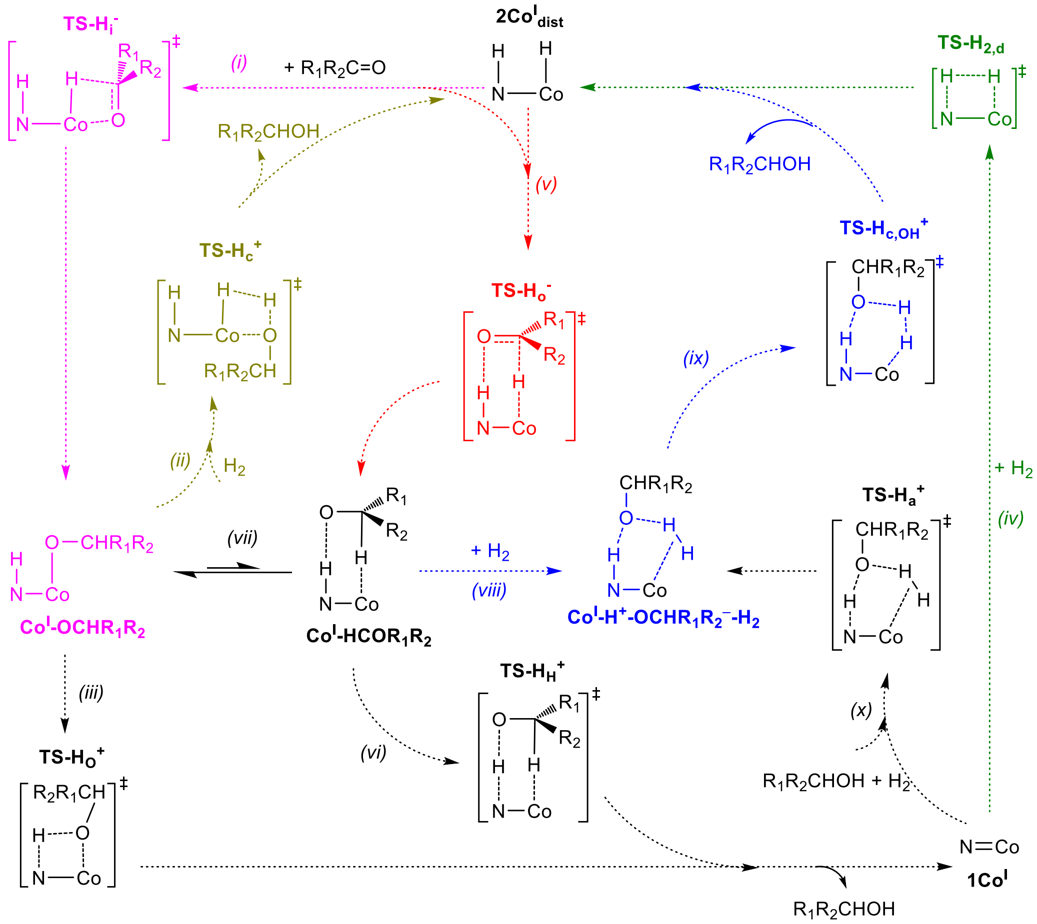

mol) and the same is also found for MECP2 (18.8 vs 21.8 kcal/mol).

The minimum energy path shows that the highest point on the Gibbs free energy profile is 115.7 kJ/mol; which is in the range of the free energy barriers of many reactions, such as the dehydrogenation of formic acid (120.3 kJ/mol),[54] transfer hydrogenation of ketone (112.4 kJ/mol),[55] and reductive amination (108 kJ/mol).[56] For using Co-based PNP catalysts, therefore, it is necessary to modify the reaction conditions (pressure and temperature) to maintain the stability of the catalysts and to adjust the reaction mechanisms for the catalytic activity and reaction selectivity. As shown in the SI (Figures S7 and S8), the stability order of these intermediates can be affected by substitution, such as chloride and methoxide instead of hydride.

Catalytic Activity of Co^{III}–, Co^I–Amine, and Amido Complexes in Carbonyl Hydrogenation. *Mechanism of Co^{III} Catalyzed C═O Hydrogenation.* For the hydrogenation of carbonyl functional groups catalyzed by the aliphatic PNP $\mathbf{2Co^{III}}$ complex, the reaction process consists of two steps, i.e., H^- transfer and H^+ transfer (Scheme 3). In the H^- transfer step (i, red line), the H^- coordinated intermediate $HCOR_1R_2^-$ [$\mathbf{Co^{III}{-}HCOR_1R_2}$] is generated via transition state $\mathbf{TS{-}H_O^-}$, and this intermediate can easily isomerize to the O-coordinated intermediate $OCHR_1R_2^-$ [$\mathbf{Co^{III}{-}OCHR_1R_2}$] (ii). Next, the H^+ transfer step has two possible routes, i.e., the innocent or the stepwise noninnocent mechanism. In the H-bonding stabilized innocent mechanism (iii, blue line), H_2 is first coordinated to the metal center forming intermediate $\mathbf{Co^{III}{-}H^+{-}OCHR_1R_2^-{-}H_2}$. Next, the regeneration of $\mathbf{2Co^{III}}$ and the release of alcohol can occur via the six-membered-ring transition state $\mathbf{TS{-}H_{c,OH}^+}$ (iv), where the N–H group stabilizes the transition state through the H-bonding. In this case, $\mathbf{2Co^{III}}$ is the real catalyst and $\mathbf{1Co^{III}}$ is off-cycle species for innocent mechanism. In the noninnocent mechanism, the H^+ transfer and H_2 addition are in stepwise fashion rather than simultaneous. First, the H^+ transfer starts from transition state $\mathbf{Co^{III}{-}OCHR_1R_2(TS{-}H_O^+)}$ (v) or from transition state $\mathbf{Co^{III}{-}HCOR_1R_2(TS{-}H_H^+)}$ (vi) forming alcohol (R_1R_2CHOH) and amido complex of $\mathbf{1Co^{III}}$. Starting from the amido complex $\mathbf{1Co^{III}}$, there are two possible ways to regenerate $\mathbf{2Co^{III}}$. One is the direct H_2 addition to $\mathbf{1Co^{III}}$ via transition state $\mathbf{TS{-}H_{2,d}}$ (vii, green line), which is a direct addition pathway of the noninnocent mechanism. The other one is the ROH assisted pathway of the noninnocent mechanism (viii), in which alcohol assists the stepwise H^+ transfer from alcohol to the amido N via transition state $\mathbf{TS{-}H_a^+}$ generating intermediate $\mathbf{Co^{III}{-}H^+{-}OCHR_1R_2^-{-}H_2}$. The next step (iv) is the heterolytic cleavage of H_2 via transition state $\mathbf{TS{-}H_{c,OH}^+}$ along with alcohol release and $\mathbf{2Co^{III}}$ regeneration. It is noted that the transition state $\mathbf{TS{-}H_{c,OH}^+}$ for $\mathbf{2Co^{III}}$ regeneration is also the second H^+ transfer step of H-bonding stabilized innocent mechanism (iii).

Mechanisms of Co^I Catalyzed C═O Hydrogenation. Different from the 18-electron $\mathbf{2Co^{III}}$ complex, the monohydride complex $\mathbf{2Co^I}$ has a vacant site for substrate coordination, and therefore the H^- transfer can occur via outer-sphere ($\mathbf{TS{-}H_O^-}$) or inner-sphere ($\mathbf{TS{-}H_i^-}$) manners (Scheme 4). After the H^- transfer step, the H^+ transfer can occur

https://doi.org/10.1021/acscatal.0c05562
ACS Catal. 2021, 11, 4593–4605

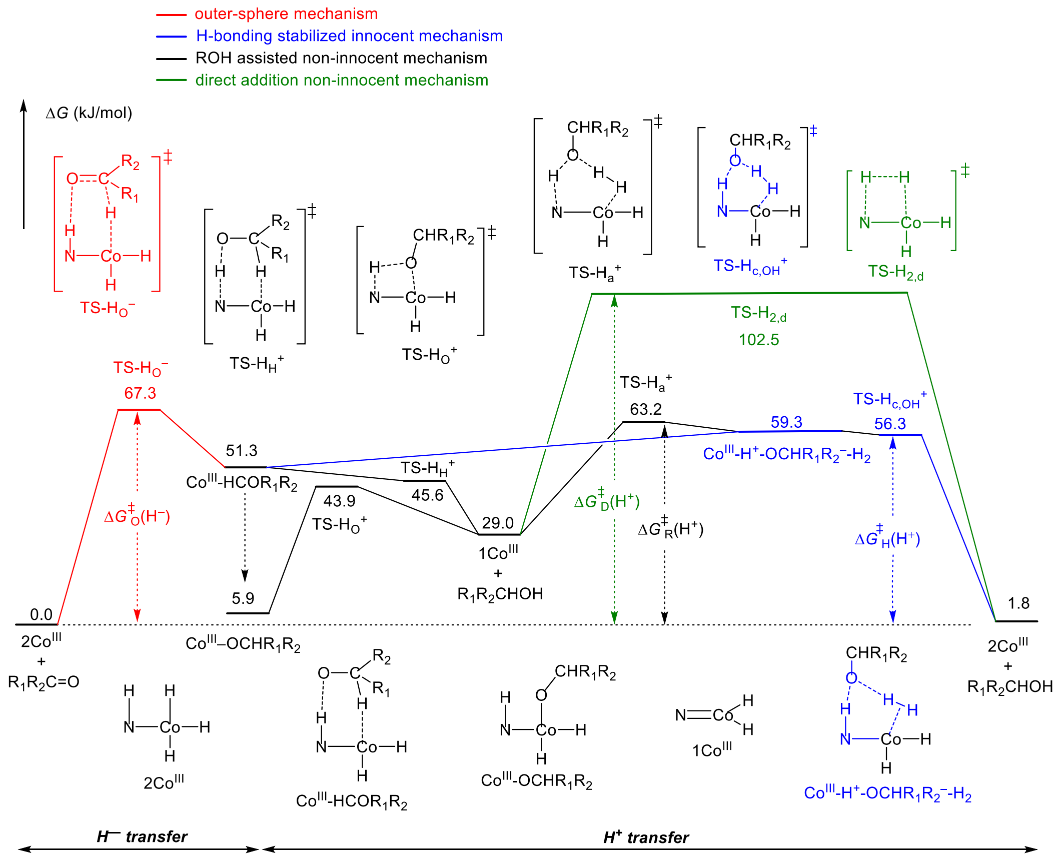

Figure 2. Gibbs free energy profile of $\mathbf{2Co^{III}}$ catalyzed $PhCOCH_3$ hydrogenation.

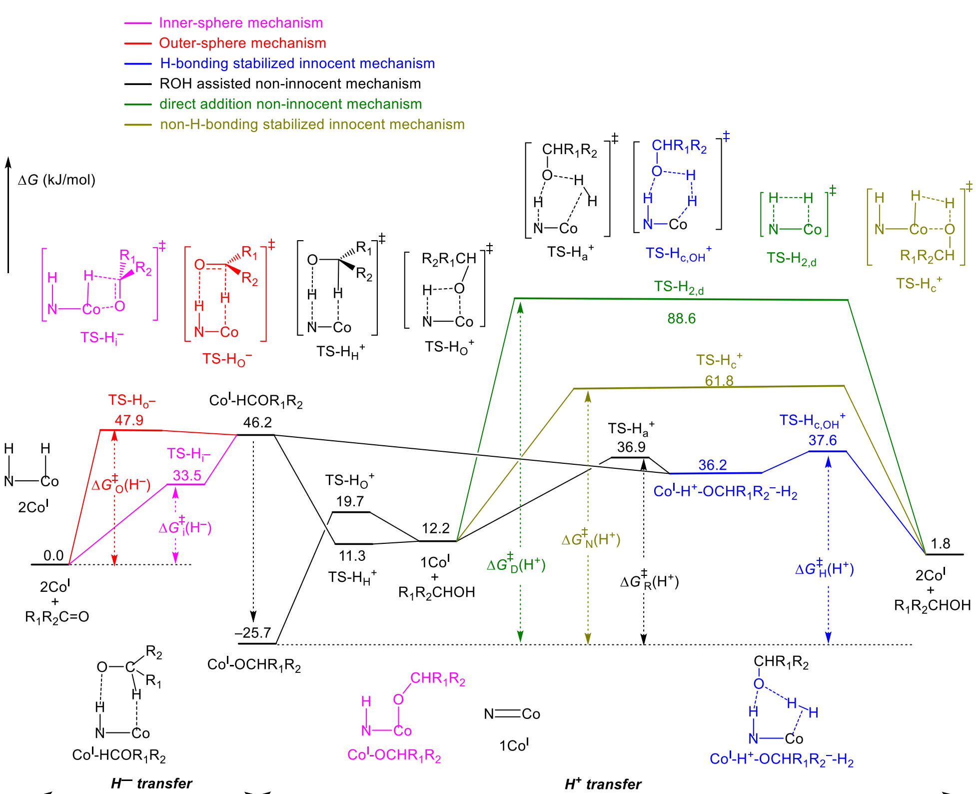

Figure 3. Gibbs free energy profile of $\mathbf{2Co^{I}}$ catalyzed $PhCOCH_3$ hydrogenation.

via the innocent or the stepwise noninnocent mechanisms. In the inner-sphere mechanism (i, purple line), the H^- insertion from Co−H to the carbon of the C═O bond via transition state of $\mathbf{TS{-}H_i^-}$ forms the O coordinated intermediate $\mathbf{Co^I}$−

https://doi.org/10.1021/acscatal.0c05562
ACS Catal. 2021, 11, 4593−4605

Table 1. Gibbs Free Energy Barrier (kJ/mol) for All Substrates Catalyzed by $2Co^{III}$

	H^- transfer	H^+ transfer		
$\Delta G^{\neq}$(kJ/mol)	outer-sphere	direct addition noninnocent	ROH assisted noninnocent	H-bonding stabilized innocent
	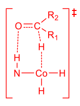	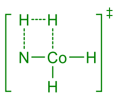	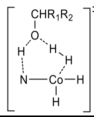 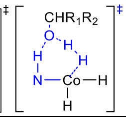	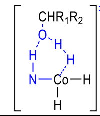
CH_2O	14.0	107.1	73.9	70.8
PhCHO	30.7	117.9	68.5	68.5
CH_3COCH_3	69.2	99.4	70.0	70.0
$PhCOCH_3$	67.3	102.5	63.2	56.3
$PhCOOCH_3$	102.0	157.6	102.8	90.6

$\mathbf{OCHR_1R_2}$. In the outer-sphere mechanism (v, red line), the H^- transfer via transition state of $\mathbf{TS\text{-}Ho^-}$ forms the H coordinated intermediate $\mathbf{Co^I{-}HCOR_1R_2}$, which can readily convert to the O coordinated intermediate $\mathbf{Co^I{-}OCHR_1R_2}$ (vii).

Both innocent and noninnocent mechanisms are considered in the H^+ transfer step. In the H-bonding stabilized innocent mechanism (blue line), H_2 firstly coordinates to the metal center forming the intermediate $\mathbf{Co^I{-}H^+{-}OCHR_1R_2^-{-}H_2}$ (viii) and the coordinated H_2 undergoes concerted heterolytic cleavage (ix), and the corresponding proton transfer via transition state of $\mathbf{TS\text{-}H_{c,OH}^+}$ results in the release of alcohol and the regeneration of $\mathbf{2Co^I}$. Since the vacant site is available for $\mathbf{Co^I{-}OCHR_1R_2}$, σ-bond metathesis of H_2 via the four-membered-ring transition state $\mathbf{TS{-}H_c^+}$, which is the non-H-bonding stabilized innocent mechanism (ii, brown line), is also considered.

In the noninnocent mechanism, the H^+ transfer can also occur from transition state $\mathbf{Co^I{-}OCHR_1R_2(TS{-}H_O^+)}$ (iii) or transition state $\mathbf{Co^I{-}HCOR_1R_2(TS{-}H_H^+)}$ (vi) along with the generation of alcohol (R_1R_2CHOH) and the amido complex $\mathbf{1Co^I}$. From the amido complex $\mathbf{1Co^I}$, $\mathbf{2Co^I}$ can be regenerated through two possible routes; the noninnocent mechanism through H_2 oxidation addition to $\mathbf{1Co^I}$ via transition state $\mathbf{TS{-}H_{2,d}}$ (iv, green line), and the ROH assisted noninnocent mechanism (x), in which the proton of alcohol shifts to N of $\mathbf{1Co^I}$ via transition state $\mathbf{TS{-}H_a^+}$. Following the transition state $\mathbf{TS{-}H_a^+}$, $\mathbf{2Co^I}$ is regenerated via intermediate $\mathbf{Co^I{-}H^+{-}OCHR_1R_2^-{-}H_2}$ and transition state $\mathbf{TS{-}H_{c,OH}^+}$. It is noted that the transition state $\mathbf{TS{-}H_{c,OH}^+}$ is the vital step for both H-bonding stabilized innocent and ROH assisted noninnocent mechanism (ix).

Catalytic Activity of CH_2O, PhCHO, CH_3COCH_3, $PhCOCH_3$, and $PhCOOCH_3$ Hydrogenation. On the basis of the proposed reaction mechanisms in Schemes 3 and 4, we computed the hydrogenation of CH_2O, PhCHO, CH_3COCH_3, $PhCOCH_3$, and $PhCOOCH_3$ using both Co^{III} and Co^I catalysts. The full Gibbs free energy profiles for each substrate are shown in the SI (Figures S9−S18), and there are in total 10 such Gibbs free energy profiles. Due to their high similarities, the full Gibbs free energy profiles of $PhCOCH_3$ hydrogenation (R_1 = Ph, R_2 = CH_3) are discussed in Figures 2 and 3.

For the $\mathbf{2Co^{III}}$ catalyzed hydrogenation of $PhCOCH_3$ (Figure 2), the Gibbs free energy barrier of the H^- transfer step, ($\Delta G^{\ddagger}_{O}(H^-)$, red line), defined as the energy difference between $\mathbf{TS{-}H_O^-}$ and the sum of $\mathbf{2Co^{III}}$ and $PhCOCH_3$, is 67.3 kJ/mol. For the hydrogenation of PhCHO, CH_3COCH_3, and $PhCOOCH_3$, the reference point of the H^- transfer step is the sum of $\mathbf{2Co^{III}}$ and the corresponding $R_1R_2C{=}O$. While for CH_2O hydrogenation, a slightly more stable coordinated structure $\mathbf{2Co^{III}\_CH_2O}$ is found to be the starting point of the H^- transfer step (Figure S9)

For $PhCOCH_3$ hydrogenation, the sum of $\mathbf{2Co^{III}}$ and $PhCOCH_3$ is defined as the reference level in the H^+ transfer step. The Gibbs free energy barrier of the H^+ transfer step via the direct addition noninnocent mechanism ($\mathbf{TS{-}H_{2,d}}$, green line) and the ROH assisted noninnocent mechanism ($\mathbf{TS{-}H_a^+}$, black line), defined as $\Delta G‡_D(H^+)$ and $\Delta G‡_R(H^+)$, is 102.5 and 63.2 kJ/mol, respectively. For the H-bonding stabilized innocent mechanism (blue line) via $\mathbf{TS{-}H_{c,OH}^+}$, the energy barrier ($\Delta G‡_H(H^+)$), defined as the difference between $\mathbf{TS{-}H_{c,OH}^+}$ and the sum of $\mathbf{2Co^{III}}$ and $PhCOCH_3$, is 56.3 kJ/mol. In addition, the reference point of the hydrogenation of CH_3COCH_3 and $PhCOOCH_3$ in the H^+ transfer step is the same as that of $PhCOCH_3$. Whereas $\mathbf{Co^{III}{-}OCHR_1R_2}$ is the reference state in the H^+ transfer step for the hydrogenation of aldehydes (Figures S9 and S11). The value of $\mathbf{TS{-}H_a^+}$ is equal and smaller than that of $\mathbf{TS{-}H_{c,OH}^+}$ for the hydrogenation of PhCHO (Figure S11) and CH_3COCH_3 (Figure S13), and those two transition states participate in the ROH assisted noninnocent pathway. Thus, we choose the higher energy of $\mathbf{TS{-}H_{c,OH}^+}$ to calculate the $\Delta G‡_R(H^+)$. Therefore, the ROH assisted noninnocent mechanism is competitive with the H-bonding stabilized innocent mechanism for the hydrogenation of PhCHO (68.5 vs 68.5 kJ/mol) and CH_3COCH_3 (70.0 vs 70.0 kJ/mol) (Table 1). All Gibbs free energy barriers of the hydrogenation of these substrates catalyzed by $\mathbf{2Co^{III}}$ are shown in Table 1.

For the Co^{III} catalyzed reactions (Table 1), the rate-determining step of CH_2O and PhCHO hydrogenation is the H^+ transfer (70.8 and 68.5 kJ/mol, respectively), while that of $PhCOCH_3$ and $PhCOOCH_3$ hydrogenation is the H^- transfer (67.3 and 102.0 kJ/mol, respectively). For CH_3COCH_3 hydrogenation, the energy barriers of H^- and H^+ transfer are very close (69.2 vs 70.0 kJ/mol). For the H^+ transfer step, it is noted that the direct H_2 addition noninnocent mechanism has the highest barrier (107.1, 117.9, 99.4, 102.5, and 157.6 kJ/mol, respectively) and is least favorable. The H-bonding stabilized innocent mechanism is the most favorable pathway for all tested substrates in H^+ transfer step.

Compared with the Co^{III} catalytic cycle, Figure 3 displays two new reaction pathways catalyzed by $\mathbf{2Co^I}$. One is in the H^- transfer step for the $PhCOCH_3$ hydrogenation via inner-sphere mechanism (purple line), and $\Delta G^{\ddagger}_{i}(H^-)$ is the energy difference between $TS{-}H_i^-$ (33.5 kJ/mol) and the sum of **2CoI** and $PhCOCH_3$ (0.0 kJ/mol). Another one undergoes the H^+ transfer step via the non-H-bonding stabilized innocent mechanism ($\Delta G^{\ddagger}_{N}(H^+)$, brown line), and the barrier (87.5 kJ/mol) is the energy difference between $\mathbf{TS{-}H_c^+}$ (61.8 kJ/mol) and the reference state $\mathbf{Co^I{-}OCHR_1R2}$ (−25.7 kJ/mol).

https://doi.org/10.1021/acscatal.0c05562
ACS Catal. 2021, 11, 4593−4605

Table 2. Gibbs Free Energy Barrier for All Substrates Catalyzed by 2Co^{I}

$\Delta G^{\neq}$ (kJ/mol)	H^- transfer		H^+ transfer			
	outer-sphere	inner-sphere	direct addition noninnocent	ROH assisted noninnocent	H-bonding stabilized innocent	non-H-bonding stabilized innocent
	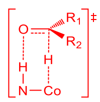	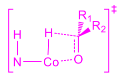	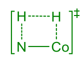	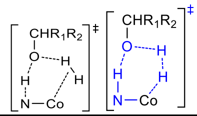	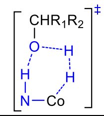	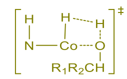
CH_2O	31.4	13.6	105.2	61.9	54.0	92.4
PhCHO	45.1	25.8	118.3	63.0	60.9	93.4
CH_3COCH_3	54.6	58.1	106.3	65.3	59.3	89.2
$PhCOCH_3$	47.9	33.5	114.3	63.3	63.3	87.5
$PhCOOCH_3$	86.0	83.1	145.7	85.9	72.1	94.6

The energy barrier of the hydride transfer catalyzed by **2Co^{I}** via inner-sphere ($\Delta G^{\ddagger}{}_{i}(H^-)$) and outer-sphere ($\Delta G^{\ddagger}{}_{O}(H^-)$) mechanisms for $PhCOCH_3$ hydrogenation relative to the starting point (sum of **2Co^{I}** and $PhCOCH_3$) is 33.5 and 47.9 kJ/mol, respectively. The sum of **2Co^{I}** and the corresponding $R_1R_2C{=}O$ is the reference state of the H^- transfer step for the hydrogenation of CH_3COCH_3 and $PhCOOCH_3$. For the hydrogenation of aldehydes, we found that there exists a more favorable coordinated structure of **2Co^{I}_$R_1R_2C{=}O$** (Figures S10 and S12), which is the real reference point of the H^- transfer step. For the H^- transfer, the inner-sphere mechanism is more preferred than the outer-sphere mechanism, except for CH_3COCH_3 (Table 2).

For $PhCOCH_3$ hydrogenation, the reference point of the H^+ transfer is **Co^{I}−$OCHR_1R_2$**, and this is different from the Co^{III}-catalyzed hydrogenation. The Gibbs free energy barrier for the H^+ transfer via the corresponding transition state, $\Delta G^{\ddagger}{}_{H}(H^+)$ (blue line), $\Delta G^{\ddagger}{}_{N}(H^+)$ (brown line) and $\Delta G^{\ddagger}{}_{D}(H^+)$ (green line) is 63.3, 87.5, and 114.3 kJ/mol, respectively. The Gibbs free energy barrier for the H^+ transfer via the transition state **TS−$H_{c,OH}{}^{+}$** of the ROH assisted noninnocent route ($\Delta G^{\ddagger}{}_{R}(H^+)$, black line) is 63.3 kJ/mol, the same as that via the transition state $\Delta G^{\ddagger}{}_{H}(H^+)$ (blue line); and both routes should be competitive. All Gibbs free energy barriers of the hydrogenation of these substrates catalyzed by **2CoI** are shown in Table 2, where the reference level for H^+ transfer is **Co^{I}−$OCHR_1R_2$** for all substrates. It shows that H^+ transfer is the rate-determining step for the hydrogenation of CH_2O (54.0 kJ/mol), PhCHO (60.9 kJ/mol), CH_3COCH_3 (59.3 kJ/mol), and $PhCOCH_3$ (63.3 kJ/mol) via the H-bonding stabilized innocent mechanism, and both direct H_2 addition noninnocent and non-H-bonding innocent mechanisms are unfavorable. On the contrary, H^- transfer is the rate-determining step for $PhCOOCH_3$ hydrogenation via an inner-sphere mechanism (83.1 kJ/mol)

It is clear that the catalytic cycle based on **2Co^{I}** is kinetically more favorable than that of **2Co^{III}** by 16.8, 7.6, 10.7, 4.0, and 18.9 kJ/mol for CH_2O, PhCHO, CH_3COCH_3, $PhCOCH_3$, and $PhCOOCH_3$, respectively.

It is interesting to compare our results with those reported previously. For the hydrogenation of $PhCOCH_3$ catalyzed by **2Co^{I}**, Qi et al., reported the H^+ transfer via direct H_2 addition noninnocent pathway as the rate-determining step (122.1 kJ/mol),[57] which is close to our value of 114.3 kJ/mol for the same pathway. While our results show that the H-bonding stabilized innocent mechanism has much lower barrier of 63.3 kJ/mol and is the rate-determining step, and this is reasonable and compatible with the reaction condition at room temperature and low H_2 pressure. It is also noted that the hydrogenation mechanisms of $PhCOOCH_3$ and PhCHO using **2Co^{III}** are different from those previously reported for the corresponding Fe-PNP pincer catalyst.[58] For $PhCOOCH_3$ hydrogenation using **2Co^{III}** as catalyst, the first step H^- transfer is the rate-determining step, while Fe-PNP catalyzed $PhCOOCH_3$ hydrogenation has the H−O dissociation of the formed hemiacetal $PhCH(OH)(OCH_3)$ as the rate-determining step. In addition, both mechanisms differ also in intermediates and transition states. For PhCHO hydrogenation, **2Co^{III}** has the H^+ transfer step via H-bonding stabilized innocent mechanism as the rate-determining step, while Fe-PNP has the first H^- transfer as the rate-determining step. On the contrary for using **2Co^{I}** as catalyst, $PhCOOCH_3$ hydrogenation prefers an inner-sphere mechanism with the first H^- transfer as the rate-determining step and PhCHO hydrogenation prefers an inner-sphere mechanism with the H^+ transfer step via H-bonding stabilized innocent mechanism as the rate-determining step.

Correlation between Hydride Affinity, Proton Affinity, and Deprotonation Gibbs Free Energy and Energy Barriers. To estimate the relationship between Gibbs free energy barriers and the strength of H^-/H^+ in reactant and product, some related parameters of catalyst, substrate, and product were calculated. We used the Gibbs free energy barrier of H^+ transfer via H-bonding stabilized innocent mechanism, as $\Delta G^{\ddagger}(H^+)$, and the Gibbs free energy barrier of H^- transfer step via outer-sphere mechanism catalyzed by **2Co^{III}** and via inner-sphere mechanism catalyzed by **2Co^{I}**, as ΔG‡(H^-), for our discussion. Generally, ΔG_{H^-} (hydricity), the opposite of energy difference between compound $[M-H]$ and its dehydrided form $[M^+ + H^-]$ ($\Delta G_{H^-}(M-H) = G[M^+] + G[H^-] - G[M-H]$), is used to describe the ability to donate/accept hydride, where smaller hydricity value means more hydridic.[59] It is found that the hydricity of **2Co^{I}** and **2Co^{III}** is 292.8 and 369.8 kJ/mol, respectively, and the **2Co^{I}** is more hydridic than **2Co^{III}**, and this can match and rationalize the lower Gibbs free energy barrier of the H^- transfer for **2Co^{I}** catalyzed hydrogenation reactions. However, it is found that large hydricity difference $\Delta\Delta G_{H^-}$ (Co^{III}/Co^{I}) = 77.0 kJ/mol results in small difference in $\Delta\Delta G^{\ddagger}(H^-, Co^{III}/Co^{I})$ (0.4, 4.9, 14.6, 33.8, and 18.9 kJ/mol for CH_2O, PhCHO, CH_3COCH_3, $PhCOCH_3$, and $PhCOOCH_3$, respectively). The similar Gibbs free energy barrier of H^- transfer for CH_2O hydrogenation is due to the more exergonic coordination of CH_2O to the vacant site of **2Co^{I}** (14.6 vs 7.7 kJ/mol for **2Co^{I}** and **2Co^{III}**, respectively), and this increases the Gibbs free energy barrier. This drives us to explore whether there exists correlation between $\Delta G^{\ddagger}(H^-)$ and hydride affinity of substrate $\Delta G_{H^-}(S) = G[S-H^-] - G[S] - G[H^-]$, where H^- is added to the carbon center of the carbonyl group resulting in alkoxide $R_1R_2CHO^-$.

https://doi.org/10.1021/acscatal.0c05562
ACS Catal. 2021, 11, 4593−4605

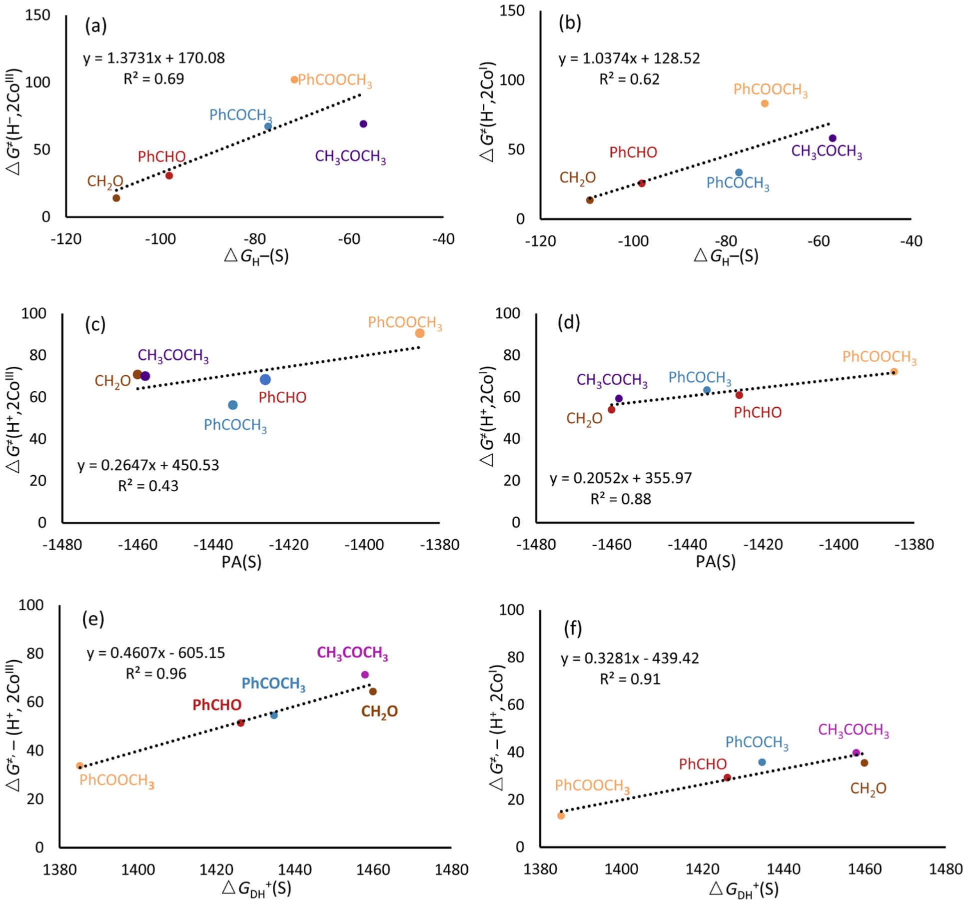

Figure 4. Correlation between $\Delta G^{\ddagger}$ for hydride transfer and hydride affinity of substrate catalyzed by **2Co^{III}** (a) and **2Co^{I}** (b); $\Delta G^{\ddagger}$ for proton transfer and PA value of $R_1R_2CHO^-$ form of product alcohols catalyzed by **2Co^{III}** (c) and **2Co^{I}** (d) as well as $\Delta G^{\ddagger}$ of alcohol deprotonation and deprotonation ΔG of alcohol (R_1R_2CHOH) catalyzed by **2Co^{III}** (e) and **2Co^{I}** (f).

As shown in Figure 4a, poor correlation between the hydride affinity of substrate and activation energy of the H^- transfer step catalyzed by **2Co^{III}** is found (R^2 = 0.69); and even worse correlation is found between the hydride affinity of substrate and activation energy of H^- transfer step catalyzed by **2Co^{I}** via inner-sphere mechanism (R^2 = 0.62, Figure 4b). Large deviation has been found for $PhCOOCH_3$ and excluding $PhCOOCH_3$ gives excellent correlation for both **2Co^{III}** and **2Co^{I}** cycles (R^2 = 0.89 and 0.95, respectively, Figure S19). Such linear correlation can evaluate the relative energy barrier in the H^- transfer step based on the hydride affinity of aldehydes and ketones.

To understand the strong deviation of $PhCOOCH_3$, we applied the ASM (activation strain model) analysis[60] to hydride transfer step of $PhCOCH_3$ and $PhCOOCH_3$ (Scheme S1 and Table S3). It is found that the distortion energies of catalyst ΔE(cat) and substrate ΔE(sub) of **TS−H$_i$$^-$** for $PhCOOCH_3$ hydrogenation catalyzed by **2Co^{I}** are 27.6 and 18.5 kJ/mol higher than those for $PhCOCH_3$, as well as ΔE(cat) and ΔE(sub) of **TS−H$_O$$^-$** for $PhCOOCH_3$ hydrogenation catalyzed by **2Co^{III}** are 14.0 and 16.0 kJ/mol higher than those for $PhCOCH_3$.

For the H^+ transfer, the proton affinity (PA) of alkoxide $R_1R_2CHO^-$ form of alcohol (PA = $G[R_1R_2CHOH] - G[R_1R_2CHO^-]$) correlates with $\Delta G^{\ddagger}(H^+)$ via the H-bonding stabilized innocent mechanism. As shown in Figure 4c,d, the PA value of $R_1R_2CHO^-$ form of product alcohols and $\Delta G^{\ddagger}(H^+)$ via H-bonding stabilized innocent mechanism is poor for **2Co^{III}** catalyzed hydrogenation (R^2 = 0.43) and good for **2Co^{I}** catalyzed reaction (R^2 = 0.88). The poor correlation can be attributed to the different stability of the **Co^{III}−OCHR$_1$R$_2$** which strongly influences the $\Delta G^{\ddagger}(H^+)$ of H-bonding stabilized innocent mechanism. Alternatively, the correlation between the deprotonation Gibbs free energy of alcohol ($\Delta G_{DH^+} = G[R_1R_2CHO^-] - G[R_1R_2CHOH]$) and the reverse reaction of alcohol deprotonation $\Delta G^{\ddagger,-}(H^+)$ (determined by **TS−H$_{c,OH}$$^+$** for **2Co^{III}** and **2Co^{I}**) was investigated in Figure 4e and Figure 4f. For the reverse reaction of alcohol deprotonation, excellent correlation is found for **2Co^{III}** (R^2 = 0.96) and **2Co^{I}** (R^2 = 0.91). The good relationship between the deprotonation Gibbs free energy of alcohol and reverse barrier $\Delta G^{\ddagger,-}(H^+)$ indicates that the energy of transition state (**TS−H$_{c,OH}$$^+$**) of H^+ transfer can be estimated by the reverse reaction of alcohol deprotonation.

Relationship between Co^{III}- and Co^{I}-Based Cycles. On the basis of the fact that the catalytic cycle of **2Co^{I}** is kinetically more favorable than that of **2Co^{III}** as well as **2Co^{I}** can be easily converted to the thermodynamically more favored **2Co^{III}** under H_2 atmosphere and given temperature, the simplified Gibbs energy profiles involving the **2Co^{I}** and **2Co^{III}** interconversion via the corresponding most favorable pathway was presented to discuss the reaction mechanisms. As shown in Figure 5, the Gibbs free energy profiles are divided into **2Co^{I}** (left) and **2Co^{III}** (right) cycles.

For the **2Co^{III}** cycle, the barrier of first step of hydride transfer (**TS−H$_O$$^-$** relative to **2Co^{III} + R$_1$R$_2$C=O**) for CH_2O (14.0 kJ/mol), PhCHO (30.7 kJ/mol), $PhCOCH_3$ (67.3 kJ/mol), and

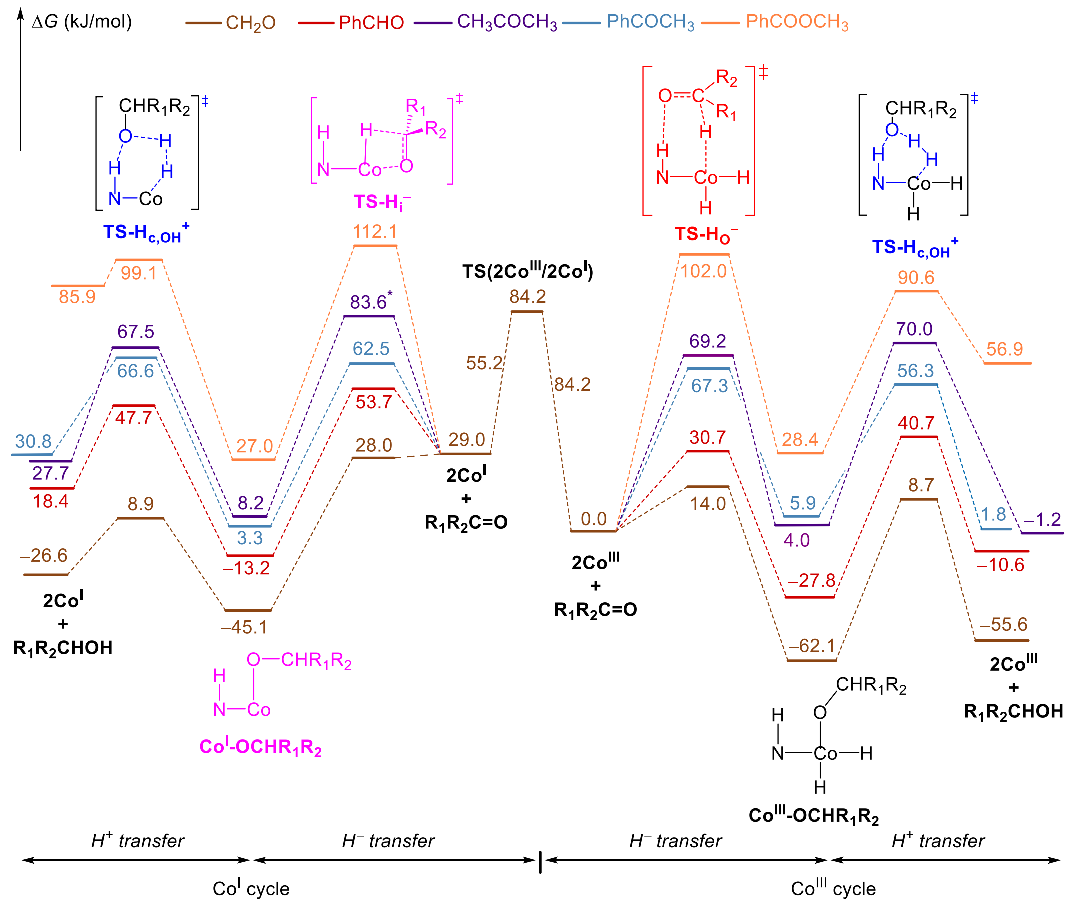

Figure 5. Most favorable Gibbs energy profile for CH_2O, PhCHO, CH_3COCH_3, $PhCOCH_3$, and $PhCOOCH_3$ hydrogenation based on Co^I/Co^{III} catalytic cycle (* for value labeled by obtained via outer-sphere mechanism).

CH_3COCH_3 (69.2 kJ/mol) to **Co^{III}−$OCHR_1R_2$** is lower than that (84.2 kJ/mol) of **$2Co^{III}$** to **$2Co^I$** conversion. The stable resting state can be found for CH_2O and PhCHO. The energy barrier of the rate-determining step of CH_2O (70.8 kJ/mol), PhCHO (68.5 kJ/mol) hydrogenation from **Co^{III}−$OCHR_1R_2$** as well as for $PhCOCH_3$ (67.3 kJ/mol) and CH_3COCH_3 (70.0 kJ/mol) hydrogenation from sum **$2Co^{III}$** and **$R_1R_2C{=}O$** is also lower than that of conversion from **$2Co^{III}$** to **$2Co^I$**, indicating that these reactions can take place at low (or even room) temperature and ambient pressure, where **$2Co^{III}$** is kept stable.

For the **$2Co^I$** cycle, the barrier of hydride transfer of CH_2O, PhCHO and $PhCOCH_3$ through **TS−H_i^-** (−1.0, 24.7, and 33.5 kJ/mol relative to **$2Co^I$** + **$R_1R_2C{=}O$**, respectively) is lower than that (55.2 kJ/mol) of **$2Co^I$** and **$2Co^{III}$** conversion. In addition, stable resting state **Co^I−$OCHR_1R_2$** (−45.1, −13.2, and 3.3 kJ/mol for CH_2O, PhCHO and $PhCOCH_3$, respectively) can be found for all substates, and the Gibbs energy relative to **$2Co^I$** + **$R_1R_2C{=}O$** is in the order of CH_2O (−74.1 kJ/mol), PhCHO (−42.2 kJ/mol), and $PhCOCH_3$ (−25.7 kJ/mol). Starting from resting state **Co^I−$OCHR_1R_2$**, the barrier of the rate-determining step of CH_2O (54.0 kJ/mol), PhCHO (60.9 kJ/mol) and $PhCOCH_3$ (63.3 kJ/mol) hydrogenation via **TS−$H_{c,OH}^+$** is lower than the intrinsic barrier of **Co^I−$OCHR_1R_2$** to **$2Co^{III}$** via **TS ($2Co^{III}$/$2Co^I$)** by 75.3, 36.5, and 17.6 kJ/mol for CH_2O, PhCHO, and $PhCOCH_3$, respectively. These indicate that these reactions also can take place at low (or even room) temperature and ambient H_2 pressure, where **$2Co^I$** is also kept stable.

Comparing the **$2Co^{III}$** and **$2Co^I$** cycles shows that both cycles can operate independently under relative low temperature and ambient H_2 pressure in which the **$2Co^I$** and **$2Co^{III}$** interconversion does not take place for CH_2O, PhCHO, and $PhCOCH_3$ hydrogenation.

For the hydrogenation of $PhCOOCH_3$ to hemiacetal on the **$2Co^{III}$** cycle, the barrier is much higher than that of the catalyst conversion from **$2Co^{III}$** to **$2Co^I$** (102.0 vs 84.2 kJ/mol), and high H_2 pressure is therefore needed to maintain the stability of **$2Co^{III}$** and high temperature is needed to overcome the barrier. The rate-determining step of hydrogenation of CH_3COCH_3 and $PhCOOCH_3$ on the **$2Co^I$** cycle is hydride transfer step via **TS−H_O^-** (83.6 kJ/mol) and via **TS−H_i^-** (112.1 kJ/mol), respectively, and their corresponding relative barriers are close (54.6 kJ/mol) or higher (83.1 kJ/mol) than that of **$2Co^I$** dehydrogenation to **$2Co^{III}$** (55.2 kJ/mol). Therefore, it is neither kinetically nor thermodynamically possible to maintain the stability of **$2Co^I$** at higher temperature under H_2 atmosphere, instead, **$2Co^I$** will be converted to **$2Co^{III}$** at first. Next, **$2Co^{III}$** participates in CH_3COCH_3 and $PhCOOCH_3$ hydrogenation and this becomes the same as found on the **$2Co^{III}$** cycle. The whole Gibbs free energy profiles in Figure 5 shows that **$2Co^{III}$** cycle is more favored kinetically (70.0 vs 83.6 kJ/mol for CH_3COCH_3 and 102.0 vs 112.1 kJ/mol for $PhCOOCH_3$) and thermodynamically (−1.2 vs 27.7 kJ/mol for CH_3COCH_3 and 56.9 vs 85.9 kJ/mol for $PhCOOCH_3$) than that of the **$2Co^I$** cycle, and this agrees with the Curtin−Hammett principle. A study of alkene hydrogenation catalyzed by bis(phosphine)cobalt dialkyl complexes revealed that reaction prefers nonredox or redox route for alkene with or without hydroxyl group.[61] Similarly, on the basis of above data, we

https://doi.org/10.1021/acscatal.0c05562
ACS Catal. 2021, 11, 4593−4605

conclude that mechanism of hydrogenation of carbonyl compounds is dependent on specific substrate.

CONCLUSIONS

For better understanding the mechanisms of hydrogenation and dehydrogenation reactions catalyzed by aliphatic PNP ligated trivalent Co^{III} and monovalent Co^{I} amine and amido complexes, we computed their structures, stability, and activation barriers in singlet, triplet, and open-shell singlet states. The Co^{III} amine and amido complexes as well as their interconversion transition state prefer singlet ground states. On the contrary, the Co^{I} amine and amido complexes as well as their interconversion transition state prefer triplet ground states. Spin exchange has been found for the interconversion from the Co^{III} amine to the Co^{I} amine complexes as well as from the Co^{III} amido to the Co^{I} amido complexes. The computed Gibbs free energy profiles show that interconversion of the trivalent Co^{III} complexes has higher barrier and is more endergonic than that of the corresponding monovalent Co^{I} complexes, and the Co^{III} complexes should prefer outer-sphere mechanisms and the Co^{I} complexes should undergo inner-sphere mechanisms.

Both innocent and noninnocent mechanisms of the hydrogenation of CH_2O, PhCHO, CH_3COCH_3, $PhCOCH_3$, and $PhCOOCH_3$ are computed. For the **2Co^{III}** catalyzed cycle, H^+ transfer is the rate-determining step for CH_2O, PhCHO, and ROH assisted noninnocent and H-bonding stabilized innocent mechanism are competitive for PhCHO hydrogenation, but the former mechanism is less favorable for CH_2O hydrogenation. For the hydrogenation of $PhCOCH_3$ and $PhCOOCH_3$, however, the rate-determining step is the H^- transfer via outer-sphere mechanism. The H^+ and H^- transfer steps have similar free energy barriers for CH_3COCH_3 hydrogenation.

For the **2Co^{I}** catalyzed cycle, H^+ transfer step is the rate-determining step for the hydrogenation of CH_2O, PhCHO, CH_3COCH_3, and $PhCOCH_3$, as well as the Gibbs energy barriers via ROH assisted noninnocent and H-bonding stabilized innocent mechanism are almost the same for PhCHO and $PhCOCH_3$, but the H-bonding stabilized innocent mechanism is more favorable for CH_2O and CH_3COCH_3. For $PhCOOCH_3$ hydrogenation, however, inner-sphere mechanism of H^- transfer is the rate-determining step. Overall, **2Co^{I}** shows better catalytic performance compared with **2Co^{III}**.

The good relationship between the hydride affinity of substrate and the barrier of H^- transfer for aldehydes, CH_2O and PhCHO, as well as ketones, CH_3COCH_3 and $PhCOCH_3$, was found. Deviation of $PhCOOCH_3$ can be rationalized by the higher distortion energies of catalyst ΔE(cat) and substrate ΔE(sub) for $PhCOOCH_3$ hydrogenation than those for $PhCOCH_3$. In addition, excellent linear correlation between the deprotonation energy of alcohol and the reverse barrier of H^+ transfer was found. These indicate that the energy of transition state of H^-/H^+ transfer via the most favorable pathway can be estimated by the hydride affinity of substrate and deprotonation energy of product.

Since the hydrogenation of CH_3COCH_3 and $PhCOOCH_3$ has close (54.6 kJ/mol) or higher (83.1 kJ/mol) barrier than that (55.2 kJ/mol) of the conversion of **2Co^{I}** to **2Co^{III}** catalysts and high temperature is needed to overcome the barriers, **2Co^{I}** is unstable and will be firstly converted to **2Co^{III}** catalyst, which is the active catalyst and the **2Co^{I}** cycle will be not accessible. All these show the substrate dependent reaction mechanisms.

ASSOCIATED CONTENT

Supporting Information

The Supporting Information is available free of charge at https://pubs.acs.org/doi/10.1021/acscatal.0c05562.

Benchmarking test (S1); full Gibbs free energy profiles including all the considered spin states with solvation effect of 1,4-dioxane and toluene (S2 and S3); data of all structures about minimum energy crossing point (MECP) on Gibbs free energy profile with solvation effect of 1,4-dioxane solvent (S4); full Gibbs free energy profile including all the considered spin states calculated with gas-phase mode (S5 and S6); comparison of the minimum path using different calculation model (S7); effect of chloro and methoxy substituents (S8 and S9); Gibbs free energy profiles of hydrogenation of carboxyl compounds catalyzed by Co^{I}-/Co^{III}-catalysts (S10−S14); linear relationship between hydride affinity of substrate and Gibbs energy barrier of hydride transfer step (S15); ASM (activation strain model) analysis for $PhCOCH_3$ and $PhCOOCH_3$ (S16); absolute energies for all optimized structures (S17−S25); Cartesian coordinates for all the optimized structures are presented (S26−S170); and impact on Gibbs free energy caused by int = superfine and int = ultrafine (S171) (PDF)

AUTHOR INFORMATION

Corresponding Authors

Zhihong Wei − *Institute of Molecular Science, Key Laboratory of Materials for Energy Conversion and Storage of Shanxi Province, Shanxi University, Taiyuan 030006, P. R. China; Leibniz-Institut für Katalyse e.V., Rostock 18059, Germany;* orcid.org/0000-0002-9460-7908; Email: weizhihong@sxu.edu.cn

Haijun Jiao − *Leibniz-Institut für Katalyse e.V., Rostock 18059, Germany;* orcid.org/0000-0002-2947-5937; Email: haijun.jiao@catalysis.de

Author

Jiali Liu − *State Key Laboratory of Coal Conversion, Institute of Coal Chemistry, Chinese Academy of Sciences, Taiyuan 030001, P. R. China; National Energy Center for Coal to Liquids, Synfuels China Company, Limited, Beijing 101400, P. R. China; University of Chinese Academy of Sciences, Beijing 100049, P. R. China*

Complete contact information is available at: https://pubs.acs.org/10.1021/acscatal.0c05562

Notes

The authors declare no competing financial interest.

ACKNOWLEDGMENTS

This work is supported by Institute of Coal Chemistry, Chinese Academy of Sciences and Synfuels China. We also thank the BMBF (Bundesministerium für Bildung und Forschung), and the State of Mecklenburg-Vorpommern in Germany for support. This work is dedicated to our colleague, Dr. Helfried Neumann, on the occasion of his 60th birthday.

REFERENCES

(1) de Vries, J. G.; Elsevier, C. J. *The Handbook of Homogenous Hydrogenation*; Wiley-VCH: Weinheim, 2006.

(2) Pritchard, J.; Filonenko, G. A.; van Putten, R.; Hensen, E. J. M.; Pidko, E. A. Heterogeneous and homogeneous catalysis for the hydrogenation of carboxylic acid derivatives: history, advances and future directions. *Chem. Soc. Rev.* **2015**, *44*, 3808−3833.
(3) Ai, W. Y.; Zhong, R.; Liu, X. F.; Liu, Q. Hydride Transfer Reactions Catalyzed by Cobalt Complexes. *Chem. Rev.* **2019**, *119*, 2876−2953.
(4) Alig, L.; Fritz, M.; Schneider, S. First-Row Transition Metal (De)Hydrogenation Catalysis Based On Functional Pincer Ligands. *Chem. Rev.* **2019**, *119*, 2681−2751.
(5) Beller, M. Introduction: First Row Metals and Catalysis. *Chem. Rev.* **2019**, *119*, 2089−2089.
(6) Wei, Z. H.; Jiao, H. J. Bifunctional aliphatic PNP pincer catalysts for hydrogenation: Mechanisms and scope. *Advances in Inorganic Chemistry*; van Eldik, R., Puchta, R., Eds.; Academic Press/Elsevier, The Netherlands, Chapter 10, 2019; Vol. 73, pp 323−384.
(7) Peris, E.; Crabtree, R. H. Key factors in pincer ligand design. *Chem. Soc. Rev.* **2018**, *47*, 1959−1968.
(8) Hashiguchi, S.; Fujii, A.; Takehara, J.; Ikariya, T.; Noyori, R. ASYMMETRIC TRANSFER HYDROGENATION OF AROMATIC KETONES CATALYZED BY CHIRAL RUTHENIUM(II) COMPLEXES. *J. Am. Chem. Soc.* **1995**, *117*, 7562−7563.
(9) Blum, Y.; Czarkie, D.; Rahamim, Y.; Shvo, Y. (CYCLOPENTADIENONE)RUTHENIUM CARBONYL-COMPLEXES - A NEW CLASS OF HOMOGENEOUS HYDROGENATION CATALYSTS. *Organometallics* **1985**, *4*, 1459−1461.
(10) Chelucci, G.; Baldino, S.; Baratta, W. Recent Advances in Osmium-Catalyzed Hydrogenation and Dehydrogenation Reactions. *Acc. Chem. Res.* **2015**, *48*, 363−379.
(11) Clapham, S. E.; Hadzovic, A.; Morris, R. H. Mechanisms of the H_2-hydrogenation and transfer hydrogenation of polar bonds catalyzed by ruthenium hydride complexes. *Coord. Chem. Rev.* **2004**, *248*, 2201−2237.
(12) Filonenko, G. A.; van Putten, R.; Hensen, E. J. M.; Pidko, E. A. Catalytic (de)hydrogenation promoted by non-precious metals - Co, Fe and Mn: recent advances in an emerging field. *Chem. Soc. Rev.* **2018**, *47*, 1459−1483.
(13) Gorgas, N.; Kirchner, K. Isoelectronic Manganese and Iron Hydrogenation/Dehydrogenation Catalysts: Similarities and Divergences. *Acc. Chem. Res.* **2018**, *51*, 1558−1569.
(14) Morris, R. H. Exploiting Metal-Ligand Bifunctional Reactions in the Design of Iron Asymmetric Hydrogenation Catalysts. *Acc. Chem. Res.* **2015**, *48*, 1494−1502.
(15) Vogiatzis, K. D.; Polynski, M. V.; Kirkland, J. K.; Townsend, J.; Hashemi, A.; Liu, C.; Pidko, E. A. Computational Approach to Molecular Catalysis by 3d Transition Metals: Challenges and Opportunities. *Chem. Rev.* **2019**, *119*, 2453−2523.
(16) Zell, T.; Milstein, D. Hydrogenation and Dehydrogenation Iron Pincer Catalysts Capable of Metal Ligand Cooperation by Aromatization/Dearomatization. *Acc. Chem. Res.* **2015**, *48*, 1979−1994.
(17) Nielsen, M.; Alberico, E.; Baumann, W.; Drexler, H. J.; Junge, H.; Gladiali, S.; Beller, M. Low-temperature aqueous-phase methanol dehydrogenation to hydrogen and carbon dioxide. *Nature* **2013**, *495*, 85−89.
(18) Bornschein, C.; Werkmeister, S.; Wendt, B.; Jiao, H. J.; Alberico, E.; Baumann, W.; Junge, H.; Junge, K.; Beller, M. Mild and selective hydrogenation of aromatic and aliphatic (di)nitriles with a well-defined iron pincer complex. *Nat. Commun.* **2014**, *5* (4111), 2014.
(19) Elangovan, S.; Topf, C.; Fischer, S.; Jiao, H. J.; Spannenberg, A.; Baumann, W.; Ludwig, R.; Junge, K.; Beller, M. Selective Catalytic Hydrogenations of Nitriles, Ketones, and Aldehydes by Well-Defined Manganese Pincer Complexes. *J. Am. Chem. Soc.* **2016**, *138*, 8809−8814.
(20) Chakraborty, S.; Dai, H. G.; Bhattacharya, P.; Fairweather, N. T.; Gibson, M. S.; Krause, J. A.; Guan, H. R. Iron-Based Catalysts for the Hydrogenation of Esters to Alcohols. *J. Am. Chem. Soc.* **2014**, *136*, 7869−7872.
(21) Zuo, W.; Lough, A. J.; Li, Y. F.; Morris, R. H. Amine(imine)-diphosphine Iron Catalysts for Asymmetric Transfer Hydrogenation of Ketones and Imines. *Science* **2013**, *342*, 1080−1083.
(22) Casey, C. P.; Guan, H. R. An efficient and chemoselective iron catalyst for the hydrogenation of ketones. *J. Am. Chem. Soc.* **2007**, *129*, 5816−5817.
(23) Morris, R. H. Exploiting metal-ligand bifunctional reactions in the design of iron asymmetric hydrogenation catalysts. *Acc. Chem. Res.* **2015**, *48* (5), 1494−1502.
(24) Benito-Garagorri, D.; Kirchner, K. Modularly Designed Transition Metal PNP and PCP Pincer Complexes based on Aminophosphines: Synthesis and Catalytic Applications. *Acc. Chem. Res.* **2008**, *41*, 201−213.
(25) Elangovan, S.; Neumann, J.; Sortais, J. B.; Junge, K.; Darcel, C.; Beller, M. Efficient and selective N-alkylation of amines with alcohols catalysed by manganese pincer complexes. *Nat. Commun.* **2016**, *7*, 12641.
(26) Kallmeier, F.; Kempe, R. Manganese Complexes for (De)-Hydrogenation Catalysis: A Comparison to Cobalt and Iron Catalysts. *Angew. Chem., Int. Ed.* **2018**, *57*, 46−60.
(27) Garbe, M.; Junge, K.; Beller, M. Homogeneous Catalysis by Manganese-Based Pincer Complexes. *Eur. J. Org. Chem.* **2017**, *2017*, 4344−4362.
(28) Garduño, J. A.; García, J. J. Toward Amines, Imines, and Imidazoles: A Viewpoint on the 3d Transition-Metal-Catalyzed Homogeneous Hydrogenation of Nitriles. *ACS Catal.* **2020**, *10*, 8012−8022.
(29) Bullock, R. M.; Chen, J. G. G.; Gagliardi, L.; Chirik, P. J.; Farha, O. K.; Hendon, C. H.; Jones, C. W.; Keith, J. A.; Klosin, J.; Minteer, S. D.; Morris, R. H.; Radosevich, A. T.; Rauchfuss, T. B.; Strotman, N. A.; Vojvodic, A.; Ward, T. R.; Yang, J. Y.; Surendranath, Y. Using nature's blueprint to expand catalysis with Earth-abundant metals. *Science* **2020**, *369*, No. eabc3183.
(30) Mills, M. R.; Barnes, C. L.; Bernskoetter, W. H. Influences of Bifunctional PNP-Pincer Ligands on Low Valent Cobalt Complexes Relevant to CO_2 Hydrogenation. *Inorg. Chem.* **2018**, *57*, 1590−1597.
(31) Zhang, G. Q.; Vasudevan, K. V.; Scott, B. L.; Hanson, S. K. Understanding the Mechanisms of Cobalt-Catalyzed Hydrogenation and Dehydrogenation Reactions. *J. Am. Chem. Soc.* **2013**, *135*, 8668−8681.
(32) Junge, K.; Wendt, B.; Cingolani, A.; Spannenberg, A.; Wei, Z. H.; Jiao, H. J.; Beller, M. Cobalt Pincer Complexes for Catalytic Reduction of Carboxylic Acid Esters. *Chem. - Eur. J.* **2018**, *24*, 1046−1052.
(33) Rozenel, S. S.; Padilla, R.; Arnold, J. Chemistry of Reduced Monomeric and Dimeric Cobalt Complexes Supported by a PNP Pincer Ligand. *Inorg. Chem.* **2013**, *52*, 11544−11550.
(34) Zhang, G. Q.; Scott, B. L.; Hanson, S. K. Mild and Homogeneous Cobalt-Catalyzed Hydrogenation of C═C, C═O, and C = N Bonds. *Angew. Chem., Int. Ed.* **2012**, *51*, 12102−12106.
(35) Rozenel, S. S.; Padilla, R.; Camp, C.; Arnold, J. Unusual activation of H_2 by reduced cobalt complexes supported by a PNP pincer ligand. *Chem. Commun.* **2014**, *50*, 2612−2614.
(36) Semproni, S. P.; Hojilla Atienza, C. C.; Chirik, P. J. Oxidative addition and C-H activation chemistry with a PNP pincer-ligated cobalt complex. *Chem. Sci.* **2014**, *5*, 1956−1960.
(37) Semproni, S. P.; Milsmann, C.; Chirik, P. J. Four-Coordinate Cobalt Pincer Complexes: Electronic Structure Studies and Ligand Modification by Homolytic and Heterolytic Pathways. *J. Am. Chem. Soc.* **2014**, *136*, 9211−9224.
(38) Srimani, D.; Mukherjee, A.; Goldberg, A. F. G.; Leitus, G.; Diskin-Posner, Y.; Shimon, L. J. W.; Ben David, Y.; Milstein, D. Cobalt-Catalyzed Hydrogenation of Esters to Alcohols: Unexpected Reactivity Trend Indicates Ester Enolate Intermediacy. *Angew. Chem., Int. Ed.* **2015**, *54*, 12357−12360.
(39) Daw, P.; Chakraborty, S.; Garg, J. A.; Ben-David, Y.; Milstein, D. Direct Synthesis of Pyrroles by Dehydrogenative Coupling of Diols and Amines Catalyzed by Cobalt Pincer Complexes. *Angew. Chem., Int. Ed.* **2016**, *55* (46), 14371−14375.

(40) Mukherjee, A.; Srimani, D.; Chakraborty, S.; Ben-David, Y.; Milstein, D. Selective Hydrogenation of Nitriles to Primary Amines Catalyzed by a Cobalt Pincer Complex. *J. Am. Chem. Soc.* **2015**, *137*, 8888−8891.

(41) Daw, P.; Chakraborty, S.; Leitus, G.; Diskin-Posner, Y.; Ben David, Y.; Milstein, D. Selective N-Formylation of Amines with H_2 and CO_2 Catalyzed by Cobalt Pincer Complexes. *ACS Catal.* **2017**, *7*, 2500−2504.

(42) Pattanaik, S.; Gunanathan, C. Cobalt-catalysed selective synthesis of aldehydes and alcohols from esters. *Chem. Commun.* **2020**, *56* (53), 7345−7348.

(43) Yang, X. Z. Hydrogenation of Carbon Dioxide Catalyzed by PNP Pincer Iridium, Iron, and Cobalt Complexes: A Computational Design of Base Metal Catalysts. *ACS Catal.* **2011**, *1*, 849−854.

(44) Guo, C. H.; Yang, D. D.; Liang, M.; Zhang, X.; Jiao, H. J. Mechanistic Insights into the Chemo-Selective Dehydrogenative Silylation of Alkenes Catalyzed by Bis(imino)pyridine Cobalt Complex from DFT Computations. *ChemCatChem* **2020**, *12*, 3890−3899.

(45) Wu, S.-B.; Zhang, T.; Chung, L. W.; Wu, Y.-D. A Missing Piece of the Mechanism in Metal-Catalyzed Hydrogenation: Co(-I)/Co(0)/Co(+I) Catalytic Cycle for Co(-I)-Catalyzed Hydrogenation. *Org. Lett.* **2019**, *21* (2), 360−364.

(46) Zhang, G. Q.; Hanson, S. K. Cobalt-Catalyzed Acceptorless Alcohol Dehydrogenation: Synthesis of Imines from Alcohols and Amines. *Org. Lett.* **2013**, *15*, 650−653.

(47) Frisch, M. J.; Trucks, G. W.; Schlegel, H. B.; Scuseria, G. E.; Robb, M. A.; Cheeseman, J. R.; Scalmani, G.; Barone, V.; Petersson, G. A.; Nakatsuji, H.; Li, X.; Caricato, M.; Marenich, A. V.; Bloino, J.; Janesko, B. G.; Gomperts, R.; Mennucci, B.; Hratchian, H. P.; Ortiz, J. V.; Izmaylov, A. F.; Sonnenberg, J. L.; Williams Ding, F.; Lipparini, F.; Egidi, F.; Goings, J.; Peng, B.; Petrone, A.; Henderson, T.; Ranasinghe, D.; Zakrzewski, V. G.; Gao, J.; Rega, N.; Zheng, G.; Liang, W.; Hada, M.; Ehara, M.; Toyota, K.; Fukuda, R.; Hasegawa, J.; Ishida, M.; Nakajima, T.; Honda, Y.; Kitao, O.; Nakai, H.; Vreven, T.; Throssell, K.; Montgomery, J. A., Jr; Peralta, J. E.; Ogliaro, F.; Bearpark, M. J.; Heyd, J. J.; Brothers, E. N.; Kudin, K. N.; Staroverov, V. N.; Keith, T. A.; Kobayashi, R.; Normand, J.; Raghavachari, K.; Rendell, A. P.; Burant, J. C.; Iyengar, S. S.; Tomasi, J.; Cossi, M.; Millam, J. M.; Klene, M.; Adamo, C.; Cammi, R.; Ochterski, J. W.; Martin, R. L.; Morokuma, K.; Farkas, O.; Foresman, J. B.; Fox, D. J. *Gaussian 16*, Rev. B.01; Gaussian, Inc.: Wallingford, CT, 2016.

(48) Schafer, A.; Huber, C.; Ahlrichs, R. Fully optimized contracted Gaussian basis sets of triple zeta valence quality for atoms Li to Kr. *J. Chem. Phys.* **1994**, *100*, 5829−5835.

(49) Marenich, A. V.; Cramer, C. J.; Truhlar, D. G. Universal Solvation Model Based on Solute Electron Density and on a Continuum Model of the Solvent Defined by the Bulk Dielectric Constant and Atomic Surface Tensions. *J. Phys. Chem. B* **2009**, *113*, 6378−6396.

(50) Zhao, Y.; Truhlar, D. G. The M06 suite of density functionals for main group thermochemistry, thermochemical kinetics, noncovalent interactions, excited states, and transition elements: two new functionals and systematic testing of four M06-class functionals and 12 other functionals. *Theor. Chem. Acc.* **2008**, *120*, 215−241.

(51) Lu, T. sobMECP, http://sobereva.com/286.

(52) Harvey, J. N.; Aschi, M.; Schwarz, H.; Koch, W. The singlet and triplet states of phenyl cation. A hybrid approach for locating minimum energy crossing points between non-interacting potential energy surfaces. *Theor. Chem. Acc.* **1998**, *99*, 95−99.

(53) Baboul, A. G.; Schlegel, H. B. Improved method for calculating projected frequencies along a reaction path. *J. Chem. Phys.* **1997**, *107*, 9413−9417.

(54) Zhou, W.; Wei, Z. H.; Spannenberg, A.; Jiao, H. J.; Junge, K.; Junge, H.; Beller, M. Cobalt-Catalyzed Aqueous Dehydrogenation of Formic Acid. *Chem. - Eur. J.* **2019**, *25*, 8459−8464.

(55) Hou, C.; Jiang, J. X.; Li, Y. W.; Zhang, Z. H.; Zhao, C. Y.; Ke, Z. F. Unusual non-bifunctional mechanism for Co-PNP complex catalyzed transfer hydrogenation governed by the electronic configuration of metal center. *Dalton Trans.* **2015**, *44*, 16573−16585.

(56) Murugesan, K.; Wei, Z. H.; Chandrashekhar, V. G.; Neumann, H.; Spannenberg, A.; Jiao, H. J.; Beller, M.; Jagadeesh, R. V. Homogeneous cobalt-catalyzed reductive amination for synthesis of functionalized primary amines. *Nat. Commun.* **2019**, *10* (1), 5443−5451.

(57) Wang, J.; Wu, K.; Qi, X. Theoretical study of the ligand effect on NHC-cobalt-catalyzed hydrogenation of ketones. *Catal. Sci. Technol.* **2019**, *9*, 5315−5321.

(58) Qu, S. L.; Dai, H. G.; Dang, Y. F.; Song, C. Y.; Wang, Z. X.; Guan, H. R. Computational Mechanistic Study of Fe-Catalyzed Hydrogenation of Esters to Alcohols: Improving Catalysis by Accelerating Precatalyst Activation with a Lewis Base. *ACS Catal.* **2014**, *4*, 4377−4388.

(59) Wiedner, E. S.; Chambers, M. B.; Pitman, C. L.; Bullock, R. M.; Miller, A. J. M.; Appel, A. M. Thermodynamic Hydricity of Transition Metal Hydrides. *Chem. Rev.* **2016**, *116*, 8655−8692.

(60) Fernandez, I.; Bickelhaupt, F. M. The activation strain model and molecular orbital theory: understanding and designing chemical reactions. *Chem. Soc. Rev.* **2014**, *43* (14), 4953−4967.

(61) Morello, G.; Zhong, H.; Chirik, P.; Hopmann, K. H. Cobalt-Catalysed Alkene Hydrogenation: A Metallacycle Can Explain the Hydroxyl Activating Effect and the Diastereoselectivity. *Chem. Sci.* **2018**, *9*, 4977−4982.

https://doi.org/10.1021/acscatal.0c05562
ACS Catal. 2021, 11, 4593−4605